

IMPROVED EXACT FBP ALGORITHM FOR SPIRAL CT

ALEXANDER KATSEVICH

ABSTRACT. Proposed is a theoretically exact formula for inversion of data obtained by a spiral CT scan with a 2-D detector array. The detector array is supposed to be of limited extent in the axial direction. The main property of the formula is that it can be implemented in a truly filtered backprojection fashion. First, one performs shift-invariant filtering of a derivative of the cone beam projections, and, second, the result is back-projected in order to form an image. Compared with an earlier reconstruction algorithm proposed by the author, the new one is two times faster, requires a smaller detector array, and does not impose restrictions on how big the patient is inside the gantry. Results of numerical experiments are presented.

1. INTRODUCTION

Spiral computed tomography (CT) involves continuous data acquisition throughout the volume of interest by simultaneously moving the patient through the gantry while the x-ray source rotates. Spiral CT has numerous advantages over conventional CT and is now a standard medical imaging modality. In the past decade it became clear that spiral CT can be significantly improved if one uses two-dimensional detector arrays instead of one-dimensional ones. This led to the development of scanners with multiple detector rows. At the present time, scanners with four and eight detector rows are commercially available. It appears that as the technology advances further, scanners with even higher number of detector rows will emerge. On the other hand, accurate and efficient image reconstruction from the data provided by such scanners is very challenging because until very recently there did not exist a theoretically exact and efficient reconstruction formula. Several approaches for image reconstruction have been proposed. They can be classified into two groups: theoretically exact and approximate. See [TD00] for a recent review of available algorithms. Most of exact algorithms are based on computing the Radon transform for a given plane by partitioning the plane in a manner determined by the spiral path of the x-ray source [Tam95, Tam97, KS97, SNS⁺00]. Even though exact algorithms are more accurate, they are computationally quite intensive and require keeping considerable amount of cone beam projections in memory. Approximate algorithms are much more efficient (see e.g. [KND98, NKD98, DNK00, B⁺00, KSK00, Kat02] for several most recent techniques), but produce artifacts, which can be significant under unfavorable circumstances.

In [Kat01b, Kat01a] the first theoretically exact inversion formula of the filtered backprojection (FBP) type was proposed. The formula can be numerically implemented in two steps. First, one performs shift-invariant filtering of a derivative of

This research was supported in part by NSF grant DMS-0104033
Department of Mathematics, University of Central Florida, Orlando, FL 32816-1364
E-mail address: akatsevi@pegasus.cc.ucf.edu.

the cone beam projections, and, second, the result is back-projected in order to form an image. The price to pay for this efficient structure is that the algorithm requires an array wider than the theoretically minimum one. Also, the algorithm is applicable if radius of support of the patient inside the gantry is not too big (not greater than $\approx 0.62 \times$ radius of gantry).

In this paper we propose an improved algorithm which is still theoretically exact and of the filtered back-projection type, but has fewer drawbacks. First, in the new algorithm there is no restriction on the size of the patient as long as he/she fits inside the gantry. Second, the new algorithm requires a smaller detector array than the old one. For example, if r and R denote radius of the patient and radius of the gantry, respectively, then in the case $r/R = 0.5$ the area of the detector array required for the old algorithm is $1.93 A_{min}$, and for the new one – $1.21 A_{min}$. Here A_{min} denotes the theoretically minimal area. Third, the new algorithm is two times faster than the old one.

In Section 2 we derive the inversion formula. In Section 3 its proof is given, and in Section 4 we show that the resulting algorithm is of the FBP type and present results of three numerical experiments.

2. INVERSION FORMULAS

First we introduce the necessary notations. Let

(2.1)

$$C := \{y \in \mathbb{R}^3 : y_1 = R \cos(s), y_2 = R \sin(s), y_3 = s(h/2\pi), s \in I\}, \quad I := [a, b],$$

where $h > 0, b > a$, be a spiral, and U be an open set strictly inside the spiral:

$$(2.2) \quad \bar{U} \subset \{x \in \mathbb{R}^3 : x_1^2 + x_2^2 < r^2, a(h/2\pi) < x_3 < b(h/2\pi)\}, \quad 0 < r < R,$$

S^2 is the unit sphere in \mathbb{R}^3 , and

$$(2.3) \quad D_f(y, \Theta) := \int_0^\infty f(y + \Theta t) dt, \quad \Theta \in S^2;$$

$$(2.4) \quad \beta(s, x) := \frac{x - y(s)}{|x - y(s)|}, \quad x \in U, s \in I; \quad \Pi(x, \xi) := \{y \in \mathbb{R}^3 : (y - x) \cdot \xi = 0\},$$

that is $D_f(y, \beta)$ is the cone beam transform of f . Given $(x, \xi) \in U \times (\mathbb{R}^3 \setminus \{0\})$, let $s_j = s_j(\xi, \xi \cdot x), j = 1, 2, \dots$, denote finitely many points of intersection of the plane $\Pi(x, \xi)$ with C . Also, $\dot{y}(s) := dy/ds$.

As was shown in [D⁺97, DNK00], any point strictly inside the spiral belongs to one and only one PI segment. Recall that a PI segment is a segment of line endpoints of which are located on the spiral and separated by less than one pitch in the axial direction (see Figure 1). Let $s = s_b(x)$ and $s = s_t(x)$ denote values of the parameter corresponding to the endpoints of the PI segment containing x . We will call $I_{PI}(x) := [s_b(x), s_t(x)]$ the PI parametric interval. The part of the spiral corresponding to $I_{PI}(x)$ will be denoted $C_{PI}(x)$.

Choose any $\psi \in C^\infty([0, 2\pi])$ with the properties

$$(2.5) \quad \psi(0) = 0; \quad 0 < \psi'(t) < 1, \quad t \in [0, 2\pi].$$

Suppose s_0, s_1 , and s_2 are related by

$$(2.6) \quad s_1 = \begin{cases} \psi(s_2 - s_0) + s_0, & s_0 \leq s_2 < s_0 + 2\pi, \\ \psi(s_0 - s_2) + s_2, & s_0 - 2\pi < s_2 < s_0. \end{cases}$$

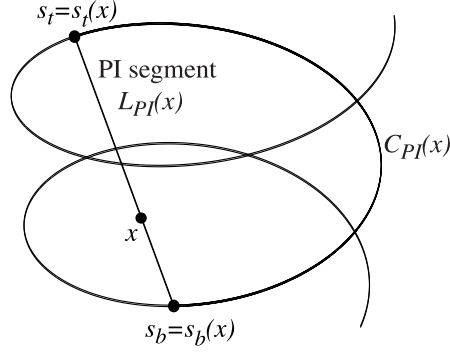


FIGURE 1. Illustration of a PI line

Since $\psi(0) = 0$, $s_1 = s_1(s_0, s_2)$ is a continuous function of s_0 and s_2 . (2.5) and (2.6) imply $s_1 \neq s_2$ unless $s_0 = s_1 = s_2$. In order to avoid unnecessary complications, we will assume in what follows

$$(2.7) \quad \psi'(0) = 0.5; \quad \psi^{(2k+1)}(0) = 0, \quad k \geq 1.$$

If (2.7) holds, then $s_1 = s_1(s_0, s_2)$ is a C^∞ function of s_0 and s_2 . Conditions (2.5) and (2.7) are very easy to satisfy. One can take, for example, $\psi(t) = t/2$, and this leads to

$$(2.8) \quad s_1 = (s_0 + s_2)/2, \quad s_0 - 2\pi < s_2 < s_0 + 2\pi.$$

Denote also

$$(2.9) \quad u(s_0, s_2) = \frac{(y(s_1) - y(s_0)) \times (y(s_2) - y(s_0))}{|(y(s_1) - y(s_0)) \times (y(s_2) - y(s_0))|} \operatorname{sgn}(s_2 - s_0), \quad 0 < |s_2 - s_0| < 2\pi,$$

$$u(s_0, s_2) = \frac{\dot{y}(s_0) \times \ddot{y}(s_0)}{|\dot{y}(s_0) \times \ddot{y}(s_0)|}, \quad s_2 = s_0.$$

Using (2.5), (2.6), and the property that $s_1 - s_0$ and $s_2 - s_0$ are always of the same sign, we find

$$(2.10) \quad u(s_0, s_2) = \frac{\dot{y}(s_0) \times \ddot{y}(s_0) + O(s_2 - s_0)}{|\dot{y}(s_0) \times \ddot{y}(s_0) + O(s_2 - s_0)|}, \quad s_2 \rightarrow s_0.$$

Hence, $u(s_0, s_2)$ is a C^∞ vector function of its arguments. Also $u(s_0, s_2) \cdot e_3 > 0$. Indeed, assume without loss of generality that $s_0 = 0$ and consider the case $0 < s_1 < s_2 < 2\pi$. Using (2.1),

$$(2.11) \quad u(s_0, s_2) \cdot e_3 = \frac{R^2}{c} [(\cos(s_1) - 1) \sin(s_2) - \sin(s_1)(\cos(s_2) - 1)]$$

$$= \frac{4R^2}{c} \sin(s_1/2) \sin(s_2/2) \sin((s_2 - s_1)/2) > 0,$$

where $c > 0$ is the denominator in (2.9). The cases $-2\pi < s_2 < s_1 < 0$ and $s_1 = s_2 = 0$ can be considered similarly.

Fix $x \in U$ and $s_0 \in I_{PI}(x)$. Find $s_2 \in I_{PI}(x)$ such that the plane through $y(s_0), y(s_2)$, and $y(s_1(s_0, s_2))$ contains x . More precisely, we have to solve for s_2 the following equation

$$(2.12) \quad (x - y(s_0)) \cdot u(s_0, s_2) = 0, \quad s_2 \in I_{PI}(x).$$

It is shown below (see (3.10) and the argument around it) that such s_2 exists, is unique, and depends smoothly on s_0 . Therefore, this construction defines $s_2 := s_2(s_0, x)$ and, consequently, $u(s_0, x) := u(s_0, s_2(s_0, x))$. Our main result is the following theorem.

Theorem 1. *For $f \in C_0^\infty(U)$ one has*

$$(2.13) \quad f(x) = -\frac{1}{2\pi^2} \int_{I_{PI}(x)} \frac{1}{|x - y(s)|} \int_0^{2\pi} \frac{\partial}{\partial q} D_f(y(q), \Theta(s, x, \gamma)) \Big|_{q=s} \frac{d\gamma}{\sin \gamma} ds,$$

where $e(s, x) := \beta(s, x) \times u(s, x)$ and $\Theta(s, x, \gamma) := \cos \gamma \beta(s, x) + \sin \gamma e(s, x)$.

Comparing (2.13) with the results of [Kat01b, Kat01a] we see that the reconstruction formula of [Kat01b, Kat01a] consists of two integrals, each of which is analogous to (2.13). Therefore, the algorithm proposed in this paper is two times faster than the older one.

Integrating by parts with respect to s in (2.13) we obtain an inversion formula in which all the derivatives are performed with respect to the angular variables.

$$(2.14) \quad \begin{aligned} f(x) = & -\frac{1}{2\pi^2} \left\{ \left[\frac{1}{|x - y(s)|} \int_0^{2\pi} D_f(y(s), \Theta(s, x, \gamma)) \frac{d\gamma}{\sin \gamma} \right] \Big|_{s=s_b(x)}^{s=s_t(x)} \right. \\ & - \int_{I_{PI}(x)} \left(\frac{\partial}{\partial s} \frac{1}{|x - y(s)|} \right) \int_0^{2\pi} D_f(y(s), \Theta(s, x, \gamma)) \frac{d\gamma}{\sin \gamma} ds \\ & - \int_{I_{PI}(x)} \frac{\beta'_s(s, x) \cdot u(s, x)}{|x - y(s)|} \int_0^{2\pi} (\nabla_{u(s, x)} D_f)(y(s), \Theta(s, x, \gamma)) \cot(\gamma) d\gamma ds \\ & - \int_{I_{PI}(x)} \frac{e'_s(s, x) \cdot u(s, x)}{|x - y(s)|} \int_0^{2\pi} (\nabla_{u(s, x)} D_f)(y(s), \Theta(s, x, \gamma)) d\gamma ds \\ & \left. - \int_{I_{PI}(x)} \frac{\beta'_s(s, x) \cdot e(s, x)}{|x - y(s)|} \int_0^{2\pi} \left(\frac{\partial}{\partial \gamma} D_f(y(s), \Theta(s, x, \gamma)) \right) \frac{d\gamma}{\sin \gamma} ds \right\}. \end{aligned}$$

Here $\beta'_s = \partial \beta / \partial s$, $e'_s = \partial e / \partial s$, and $\nabla_u D_f$ denotes the derivative of D_f with respect to the angular variables along the direction u :

$$(2.15) \quad (\nabla_u D_f)(y(s), \Theta) = \frac{\partial}{\partial t} D_f(y(s), \sqrt{1 - t^2} \Theta + tu) \Big|_{t=0}, \quad \Theta \in u^\perp.$$

3. PROOF OF THEOREM 1

Let $x \in U$ be fixed. Consider the integral with respect to γ in (2.13):

$$\begin{aligned}
& \int_0^{2\pi} \frac{\partial}{\partial q} \int_0^\infty f(y(q) + t(\cos \gamma \beta(s, x) + \sin \gamma e(s, x))) \Big|_{q=s} \frac{1}{t \sin \gamma} t dt d\gamma \\
&= \int_{\mathbb{R}^2} \frac{\partial}{\partial q} f(y(q) + u) \Big|_{q=s} \frac{1}{u \cdot e(s, x)} du \\
(3.1) \quad &= \frac{1}{(2\pi)^3} \int_{\mathbb{R}^3} \tilde{f}(\xi) \int_{\mathbb{R}^2} \frac{\partial}{\partial q} e^{-i\xi \cdot (y(q) + u)} \Big|_{q=s} \frac{1}{u \cdot e(s, x)} du d\xi \\
&= \frac{1}{(2\pi)^3} \int_{\mathbb{R}^3} \tilde{f}(\xi) (-i\xi \cdot \dot{y}(s)) e^{-i\xi \cdot y(s)} \left[\int_{\mathbb{R}} e^{-i\xi_1 u_1} du_1 \int_{\mathbb{R}} e^{-i\xi_2 u_2} \frac{du_2}{u_2} \right] d\xi \\
&= \frac{1}{(2\pi)^3} \int_{\mathbb{R}^3} \tilde{f}(\xi) (-i\xi \cdot \dot{y}(s)) e^{-i\xi \cdot y(s)} 2\pi \delta(\xi_1) (-i\pi \operatorname{sgn} \xi_2) d\xi \\
&= \frac{|x - y(s)|}{4\pi} \int_{\mathbb{R}^3} \tilde{f}(\xi) (\xi \cdot \dot{y}(s)) e^{-i\xi \cdot y(s)} \delta(\xi \cdot (x - y(s))) \operatorname{sgn}(\xi \cdot e(s, x)) d\xi.
\end{aligned}$$

Here we have assumed without loss of generality that the ξ_1 -axis is parallel to $\beta(s, x)$, and the ξ_2 -axis is parallel to $e(s, x)$. In regularizing the divergent integrals in (3.1) it is essential that $\operatorname{supp} f$ is strictly inside the spiral and separated from the ray $u_1 \leq 0, u_2 = 0$. Pick any $\delta_1 \in C_0^\infty(\mathbb{R})$, $\delta_1(t) \geq 0$, $\int \delta_1(t) dt = 1$, and define $\delta_\epsilon(t) = \epsilon^{-1} \delta_1(t/\epsilon)$. Replacing δ and sgn by δ_ϵ and $\operatorname{sgn}_\epsilon = \operatorname{sgn} * \delta_\epsilon$, respectively, in (3.1) we get

$$(3.2) \quad A(s, x) = \lim_{\epsilon \rightarrow 0^+} \int_{\mathbb{R}^3} \tilde{f}(\xi) (\xi \cdot \dot{y}(s)) \delta_\epsilon(\xi \cdot (x - y(s))) \operatorname{sgn}_\epsilon(\xi \cdot e(s, x)) e^{-i\xi \cdot y(s)} d\xi,$$

where $A(s, x)$ is the last integral in (3.1). Substituting into (2.13) we get

$$(3.3) \quad (\mathcal{B}f)(x) = \frac{1}{(2\pi)^3} \int_{I_{PI}(x)} \lim_{\epsilon \rightarrow 0^+} A_\epsilon(s, x) ds,$$

where $A_\epsilon(s, x)$ is the integral on the right in (3.2). Since it is not known at this point that the right-hand side of (2.13) equals $f(x)$, we denoted it $(\mathcal{B}f)(x)$.

Since $\tilde{f} \in \mathcal{S}(\mathbb{R}^3)$ and $x - y(s) \perp e(s, x)$, it is easy to see that $A_\epsilon(s, x)$ is uniformly bounded with respect to $s \in I_{PI}(x)$ as $\epsilon \rightarrow 0^+$. Hence, using the Lebesgue dominated convergence theorem and changing the order of integration

$$\begin{aligned}
(3.4) \quad & (\mathcal{B}f)(x) = \frac{1}{(2\pi)^3} \lim_{\epsilon \rightarrow 0^+} \int_{\mathbb{R}^3} \tilde{f}(\xi) G_\epsilon(x, \xi) d\xi, \\
& G_\epsilon(x, \xi) := \int_{I_{PI}(x)} (\xi \cdot \dot{y}(s)) \delta_\epsilon(\xi \cdot (x - y(s))) \operatorname{sgn}_\epsilon(\xi \cdot e(s, x)) e^{-i\xi \cdot y(s)} ds.
\end{aligned}$$

Clearly, $G_\epsilon(x, \xi = 0) = 0$. We will show that $|G_\epsilon(x, \xi)| < c, \xi \neq 0$, for some $c > 0$ and all $\epsilon > 0$. Indeed, let $s = q_k \in I_{PI}(x)$, $q_1 < q_2 < \dots$, be the roots of the equation $\xi \cdot \dot{y}(s) = 0$. Obviously the number of such roots is uniformly bounded

with respect to $\xi \in \mathbb{R}^3 \setminus 0$. Say, there are no more than K roots. Then,

$$(3.5) \quad \begin{aligned} |G_\epsilon(x, \xi)| &\leq \int_{I_{PI}(x)} \delta_\epsilon(\xi \cdot (x - y(s))) |\xi \cdot \dot{y}(s)| ds \\ &\leq \left(\int_{s_b}^{q_1} + \sum_{k=1}^{K-1} \int_{q_k}^{q_{k+1}} + \int_{q_K}^{s_t} \right) \delta_\epsilon(\xi \cdot (x - y(s))) (\xi \cdot \dot{y}(s)) ds \operatorname{sgn}(\xi \cdot \dot{y}(q_k^*)), \end{aligned}$$

where q_k^* is the midpoint of the corresponding interval of integration. Each term in the summation in (3.5) is bounded because

$$(3.6) \quad \begin{aligned} &\int_{q_k}^{q_{k+1}} \delta_\epsilon(\xi \cdot (x - y(s))) (\xi \cdot \dot{y}(s)) ds \operatorname{sgn}(\xi \cdot \dot{y}(q_k^*)) \\ &\leq \int_{t=\xi \cdot y(q_k)}^{t=\xi \cdot y(q_{k+1})} \delta_\epsilon(\xi \cdot x - t) dt \operatorname{sgn}(\xi \cdot \dot{y}(q_k^*)) \leq \int \delta_\epsilon(\xi \cdot x - t) dt = 1, \end{aligned}$$

and (3.5), (3.6) imply $|G_\epsilon(x, \xi)| < K + 1$.

It is clear that any plane through x intersects $C_{PI}(x)$ at least at one point. Introduce the following sets:

$$(3.7) \quad \begin{aligned} Crit(x) &= \{\xi \in \mathbb{R}^3 \setminus 0 : \Pi(x, \xi) \text{ contains } y(s_b(x)), y(s_t(x)) \text{ or} \\ &\quad \Pi(x, \xi) \text{ is tangent to } C_{PI}(x)\} \cup \{0\}, \\ \Xi_1(x) &= \{\xi \in \mathbb{R}^3 : \xi \notin Crit(x) \text{ and } \Pi(x, \xi) \cap C_{PI}(x) \text{ contains one point}\}, \\ \Xi_3(x) &= \mathbb{R}^3 \setminus \{\Xi_1(x) \cup Crit(x)\}, \\ \Xi_\psi(x) &= \{\xi \in \mathbb{R}^3 : \xi = \lambda u(s, x), s \in I_{PI}(x), \lambda \in \mathbb{R}\}. \end{aligned}$$

Recall that $u(s, x)$ was defined above Theorem 1. By construction, the sets $Crit(x)$, $\Xi_{1,3}(x)$ are pairwise disjoint, their union is all of \mathbb{R}^3 , $Crit(x)$ and $\Xi_\psi(x)$ have Lebesgue measure zero, and $\Xi_{1,3}(x)$ are open.

Take any $\xi \notin Crit(x) \cup \Xi_\psi(x)$. An easy calculation based on the change of variables $t = \xi \cdot y(s)$ as in (3.6) shows

$$(3.8) \quad \begin{aligned} \lim_{\epsilon \rightarrow 0^+} G_\epsilon(x, \xi) &= e^{-i\xi \cdot x} B(x, \xi), \\ B(x, \xi) &= \sum_{s_j \in I_{PI}(x)} \operatorname{sgn}(\xi \cdot \dot{y}(s_j)) \operatorname{sgn}(\xi \cdot e(s_j, x)). \end{aligned}$$

Recall that $s_j = s_j(\xi, \xi \cdot x)$, $j = 1, 2, \dots$, denote parameter values corresponding to points of intersection of the plane $\Pi(x, \xi)$ with the spiral and are found by solving $\xi \cdot (x - y(s)) = 0$. Here we have used that $\xi \cdot (x - y(s_j)) = 0$ implies $\xi \cdot \dot{y}(s_j) \neq 0$ and $\xi \cdot e(s_j, x) \neq 0$. Indeed, if $\xi \cdot \dot{y}(s_j) = 0$, then $\Pi(x, \xi)$ is tangent to $C_{PI}(x)$ at $y(s_j)$ and $\xi \in Crit(x)$. If $\xi \cdot e(s_j, x) = 0$, then together with $\xi \cdot \beta(s_j, x) = 0$ this implies $\xi \in \Xi_\psi(x)$. In both cases we get a contradiction. This argument implies also that $B(x, \xi)$ is locally constant in a neighborhood of any $\xi \notin Crit(x) \cup \Xi_\psi(x)$.

We now study the function $B(x, \xi)$. Recall that $x \in U$ is fixed. By construction, $G_\epsilon(x, \xi) \in C^\infty(\mathbb{R}^3)$. Since $e^{i\xi \cdot x} G_\epsilon(x, \xi) \rightarrow B(x, \xi)$, $\epsilon \rightarrow 0$, on $\mathbb{R}^3 \setminus \{Crit(x) \cup \Xi_\psi(x)\}$ and the sets $Crit(x)$, $\Xi_\psi(x)$ have Lebesgue measure zero, $B(x, \xi)$ is measurable (cf. [Lan93], p. 125). Moreover, $B(x, \xi) \in L^\infty(\mathbb{R}^3)$ because the functions $G_\epsilon(x, \xi)$ are uniformly bounded on \mathbb{R}^3 as $\epsilon \rightarrow 0$. Thus, in order to finish the proof we have to show that $B(x, \xi) = 1$ for almost all $\xi \in \mathbb{R}^3$.

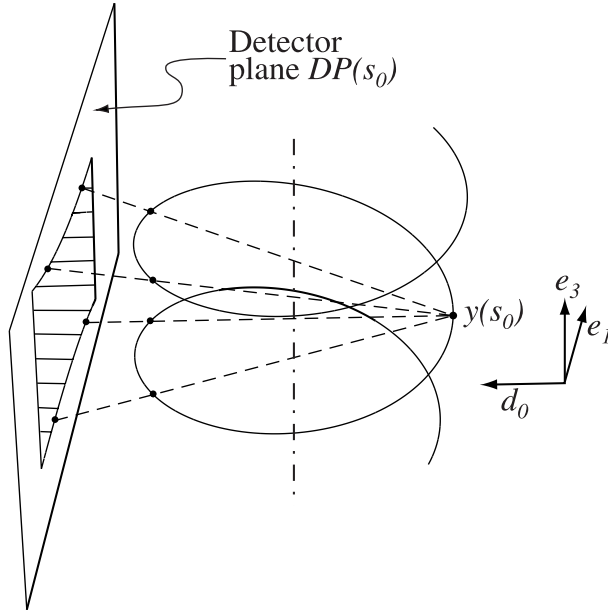


FIGURE 2. Stereographic projection from the source onto the detector plane $DP(s_0)$

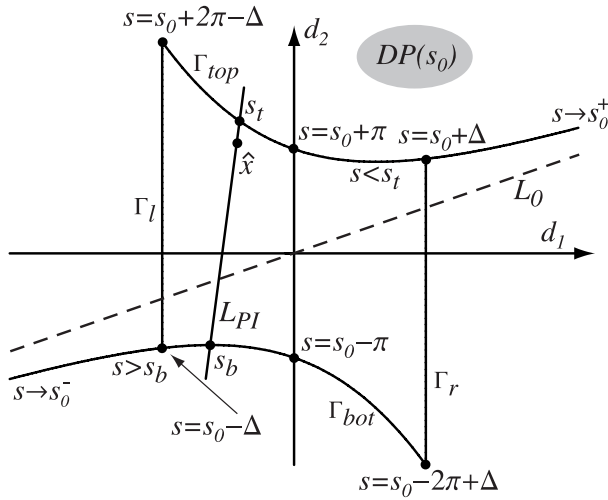


FIGURE 3. Illustration of the detector plane $DP(s_0)$

Suppose first that the x-ray source is fixed at $y(s_0)$ for some $s_0 \in I_{PI}(x)$. Project stereographically the upper and lower turns of the spiral onto the detector plane as shown in Figure 2. Since the detector array rotates together with the source, the detector plane depends on s_0 and is denoted $DP(s_0)$. It is assumed that $DP(s_0)$ is parallel to the axis of the spiral and is tangent to the cylinder $y_1^2 + y_2^2 = R^2$ (cf. (2.1)) at the point opposite to the source. Thus, the distance between $y(s_0)$ and

the detector plane is $2R$. In order to make Figure 2 more readable, the detector plane is drawn slightly away from the spiral. Introduce coordinates in the detector plane as follows. Let the d_1 -axis be perpendicular to the axis of the spiral, and the d_2 -axis be parallel to it. This gives the following parametric curves:

$$(3.9) \quad d_1(s) = 2R \frac{\sin(s - s_0)}{1 - \cos(s - s_0)}, \quad d_2(s) = \frac{h}{\pi} \frac{s - s_0}{1 - \cos(s - s_0)},$$

$$\Delta \leq s - s_0 \leq 2\pi - \Delta \text{ or } \Delta - 2\pi \leq s - s_0 \leq -\Delta,$$

where Δ is determined by the radius of support of the patient: $\Delta = 2 \cos^{-1}(r/R)$ (cf. (2.2)). The top and bottom curves are denoted Γ_{top} and Γ_{bot} , respectively (see Figure 3). Let \hat{x} denote the projection of x . Since $s_0 \in I_{PI}(x)$, \hat{x} is projected into the area between Γ_{top} and Γ_{bot} . Equations (3.9) imply that the curves Γ_{bot} and Γ_{top} are strictly convex. Also, Γ_{top} approaches L_0 from above as $s \rightarrow s_0^+$ (in this case $d_1(s) \rightarrow +\infty$), Γ_{bot} approaches L_0 from below as $s \rightarrow s_0^-$ ($d_1(s) \rightarrow -\infty$). L_0 denotes the intersection of the plane containing $y(s_0)$ and parallel to $\dot{y}(s_0), \ddot{y}(s_0)$, with the detector plane. L_{PI} denotes the intersection of the plane containing $x, y(s_0), y(s_b(x))$, and $y(s_t(x))$ with the detector plane. Note that if Γ_{bot} and Γ_{top} are intersected by a vertical line (i.e., parallel to the d_2 -axis), then the difference between values of the parameter s at the two points of intersection is exactly 2π . By assumption, $s_t(x) - s_b(x) < 2\pi$. Therefore, L_{PI} has positive slope in Figure 3.

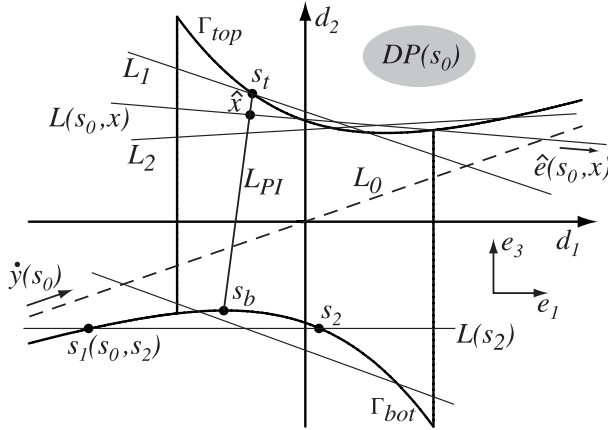


FIGURE 4. The family of lines $L(s_2)$ is shown. $L(s_0, x)$ denotes the line in that family which passes through \hat{x}

Consider a one-parametric family of planes $\Pi(s_2)$ passing through $y(s_0)$, $y(s_2)$, and $y(s_1(s_0, s_2))$. Intersections of these planes with the detector plane $DP(s_0)$ produces a family of lines $L(s_2)$ (see Figure 4). By construction, either $s_0 < s_1 < s_2$, or $s_2 < s_1 < s_0$, or $s_0 = s_1 = s_2$. Therefore, if $s_0 < s_1 < s_2$, $L(s_2)$ intersects Γ_{top} at two points. If $s_2 < s_1 < s_0$, $L(s_2)$ intersects Γ_{bot} at two points. And, by continuity, $L(s_2) = L_0$ if $s_0 = s_1 = s_2$. Suppose, for example, that \hat{x} is located above L_0 . Selecting $s_2 = s_t(x)$, it is clear that $L(s_2 = s_t(x))$ passes above \hat{x} (see line L_1 in Figure 4). On the other hand, taking s_2 sufficiently close to s_0 , $s_2 > s_0$, $L_2(s_2)$ will pass below \hat{x} (see line L_2 in Figure 4). Therefore, there exists at least one $s_2 > s_0$ such that $\hat{x} \in L(s_2)$. This line will be denoted $L(s_0, x)$. Suppose there are two

values s_2, s'_2 , $0 < s'_2 < s_2 < s_t(x)$ such that $\hat{x} \in L(s_2)$ and $\hat{x} \in L(s'_2)$. Since \hat{x} is below Γ_{top} , this implies

$$(3.10) \quad 0 < s_1 < s'_1 < s'_2 < s_2, \quad s_1 := s_1(s_0, s_2), \quad s'_1 := s_1(s_0, s'_2).$$

From (2.6), $\partial s_1 / \partial s_2 = \psi'(s_2 - s_0) > 0$, that is $s_2 > s'_2$ implies $s_1 > s'_1$, and this contradicts (3.10). Hence, there exists a unique $s_2, s_0 < s_2 < s_t(x)$, such that $x \in \Pi(s_2)$. The case when \hat{x} appears below L_0 can be considered similarly. If $\hat{x} \in L_0$, then the unique solution is $s_2 = s_0$.

To prove that $s_2 = s_2(s_0, x)$ depends smoothly on s_0 we first consider the case when s_0 is such that $s_2(s_0, x)$ and s_0 are close. According to the preceding discussion this happens when $s_0 \rightarrow \check{s}(x)$, where $\check{s}(x) \in I_{PI}(x)$ is the unique value such that the plane through $y(\check{s}(x))$ and parallel to $\dot{y}(\check{s}(x)), \ddot{y}(\check{s}(x))$ contains x . It is easily seen that such $\check{s}(x)$ exists and is unique. To simplify the notations, we can assume without loss of generality that $\check{s}(x) = 0$. Thus,

$$(3.11) \quad x = y(0) + a\dot{y}(0) + b\ddot{y}(0), \quad b > 0.$$

The condition $b > 0$ follows from $x \in U$. Taking into account terms of the first order of smallness and using (2.7), we find analogously to (2.10):

$$(3.12) \quad u(s_0, s_2) = \frac{[\dot{y}(s_0) \times \ddot{y}(s_0)] + [\dot{y}(s_0) \times \ddot{y}(s_0)] \frac{s_2 - s_0}{2} + O((s_2 - s_0)^2)}{[[\dot{y}(s_0) \times \ddot{y}(s_0)] + [\dot{y}(s_0) \times \ddot{y}(s_0)] \frac{s_2 - s_0}{2} + O((s_2 - s_0)^2)]}, \quad s_2 \rightarrow s_0.$$

Substituting (3.11) and (3.12) into (2.12), implicitly differentiating the resulting equation with respect to s_0 , and then setting $s_0 = 0$ gives

$$(3.13) \quad \{b\ddot{y}(0) \cdot (\dot{y}(0) \times \ddot{y}(0))\} \left[1 + \frac{(\partial s_2 / \partial s_0) - 1}{2} \right] = 0.$$

Since the expression in braces is not zero, we find

$$(3.14) \quad \left. \frac{\partial s_2(s_0, x)}{\partial s_0} \right|_{s_0 = \check{s}(x)} = -1.$$

Suppose now $s_0 \in (s_b(x), s_t(x))$, $s_0 \neq \check{s}(x)$. Instead of solving (2.12) for s_2 , we can find the appropriate line $L(s_2)$ in Figure 4 which contains \hat{x} . Let $(\hat{x}_1(s_0), \hat{x}_2(s_0))$ be the coordinates of \hat{x} on the detector plane $DP(s_0)$. Obviously, these coordinates depend smoothly on s_0 . Consider, for example, the case when \hat{x} appears above L_0 . Then $s_0 < s_1 < s_2$. The equation for s_2 is

$$(3.15) \quad \frac{\hat{x}_2(s_0) - d_2(s_2 - s_0)}{\hat{x}_2(s_0) - d_2(s_1 - s_0)} = \frac{\hat{x}_1(s_0) - d_1(s_2 - s_0)}{\hat{x}_1(s_0) - d_1(s_1 - s_0)}.$$

To simplify the notations, after all differentiations have been carried out the dependence of $\hat{x}_{1,2}$ on s_0 will be dropped and it will be assumed without loss of generality that $s_0 = 0$. Multiplying (3.15) out, taking into account $s_1 - s_0 = \psi(s_2 - s_0)$, and differentiating with respect to s_0 , we obtain an equation in which $\partial s_2 / \partial s_0$ is multiplied by:

$$(3.16) \quad \begin{aligned} \kappa := & d'_1(s_2)(\hat{x}_2 - d_2(s_1)) + d'_2(s_1)\psi'(s_2)(\hat{x}_1 - d_1(s_2)) \\ & - d'_2(s_2)(\hat{x}_1 - d_1(s_1)) - d'_1(s_1)\psi'(s_2)(\hat{x}_2 - d_2(s_2)). \end{aligned}$$

In view of the implicit function theorem we have to show $\kappa \neq 0$. Dividing by $\hat{x}_1 - d_1(s_1) \neq 0$ and using (3.15), transforms (3.16) to

$$(3.17) \quad d'_1(s_2) \left[\frac{\hat{x}_2 - d_2(s_2)}{\hat{x}_1 - d_1(s_2)} - \frac{d'_2(s_2)}{d'_1(s_2)} \right] + \psi'(s_2) d'_1(s_1) \frac{\hat{x}_1 - d_1(s_2)}{\hat{x}_1 - d_1(s_1)} \left[\frac{d'_2(s_1)}{d'_1(s_1)} - \frac{\hat{x}_2 - d_2(s_2)}{\hat{x}_1 - d_1(s_2)} \right].$$

Interpreting the ratios in brackets in (3.17) as slopes, we see that the two expressions in brackets are positive (cf. Figure 4). Using that $d'_1(s_{1,2}) < 0$, $\psi' > 0$, and $\hat{x}_1 > d_1(s_{1,2})$ (again cf. Figure 4), we prove $\kappa \neq 0$. κ remains bounded away from zero even if $s_0 \rightarrow s_b(x)$. In this case $\hat{x} \rightarrow \Gamma_{top}$ and, in the limit $\hat{x} = (d_1(s_2), d_2(s_2))$, where $s_2 = s_t(x)$, (3.17) becomes

$$(3.18) \quad d'_1(s_2) \left[\frac{d_2(s_2) - d_2(s_1)}{d_1(s_2) - d_1(s_1)} - \frac{d'_2(s_2)}{d'_1(s_2)} \right] < 0,$$

where we have used (3.15). The case when \hat{x} appears below L_0 can be treated similarly.

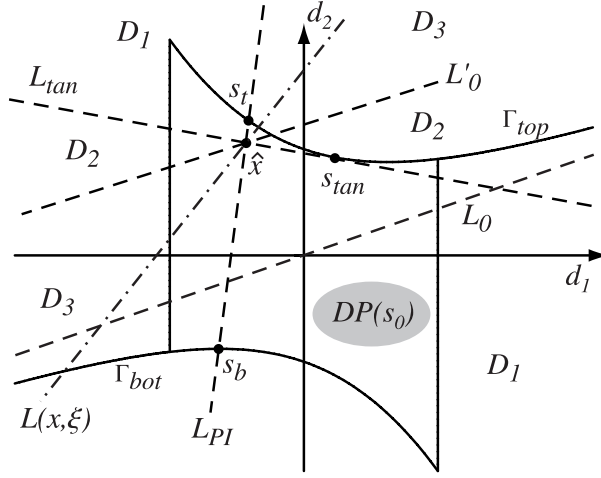


FIGURE 5. Detector plane with various lines through \hat{x} shown

Consider various lines through \hat{x} (see Figure 5). L_{tan} denotes the line through \hat{x} and tangent to either Γ_{top} if \hat{x} is above L_0 , or Γ_{bot} if \hat{x} is below L_0 . In both cases the point of tangency should fall inside the PI-parametric interval and, therefore, is unique. The corresponding parameter value will be denoted s_{tan} . If $\hat{x} \in L_0$, by continuity $L_{tan} = L_0$. L'_0 is the line through \hat{x} and parallel to L_0 . Finally, $L(x, \xi)$ is the intersection of $\Pi(x, \xi) \ni y(s_0)$ with the detector plane. Clearly, there is one-to-one correspondence between the planes $\Pi(x, \xi)$, where ξ satisfies $\xi \cdot (x - y(s_0)) = 0$, and the lines $L(x, \xi)$. The lines L_{PI} , L_{tan} , and L'_0 split the detector plane into three conical regions: $D_j, j = 1, 2, 3$. If $\hat{x} \in L_0$, then $L_{tan} = L_0$ and D_2 collapses into an empty set. If $L(x, \xi) \subset D_1$, $\Pi(x, \xi) \cap C_{PI}(x)$ contains only one point - $y(s_0)$. If $L(x, \xi) \subset D_2$, there are three points of intersection of $\Pi(x, \xi)$ with $C_{PI}(x)$. If \hat{x} is above L_0 , they correspond to values of the parameter $s = a, b, c$ that satisfy $a = s_0 < b < c < s_t(x)$. Recall that in this region the slope of $L(x, \xi)$ is smaller than that of L_0 . If \hat{x} is below L_0 the situation is essentially the same. The only

difference is that $L(x, \xi) \subset D_2$ implies that parameter values at the three points of intersection of $\Pi(x, \xi)$ with $C_{PI}(x)$ satisfy $s_b < a < b < c = s_0$. If $L(x, \xi) \subset D_3$ (an example of such a line is shown in Figure 5), then again there are three points of intersection of $\Pi(x, \xi)$ with $C_{PI}(x)$, and $s_b(x) < a < b = s_0 < c < s_t(x)$. This argument shows that if $\xi \in \Xi_1$ (i.e. when $C_{PI}(x) \cap \Pi(x, \xi)$ consists of one point), then $L(x, \xi) \subset D_1$. If $\xi \in \Xi_3$, then $C_{PI}(x) \cap \Pi(x, \xi)$ consists of precisely three points and $L(x, \xi) \subset D_2$ or D_3 .

In order to compute the value of the sum in (3.8) we need a simplifying argument. Let $\hat{\xi}$ be a nonzero vector in the detector plane $DP(s_0)$ perpendicular to $L(x, \xi)$ and pointing into the same half-space as ξ , that is $\xi \cdot \hat{\xi} > 0$. Fix any nonzero vector $e \in \mathbb{R}^3$ perpendicular to $\beta(s_0, x)$, and let L be the line in the intersection of $\Pi(x, \beta(s_0, x) \times e)$ with the detector plane. Analogously, \hat{e} denotes a vector in the detector plane parallel to L and with the property $e \cdot \hat{e} > 0$. We claim that

$$(3.19) \quad \text{sgn}(\xi \cdot e) = \text{sgn}(\hat{\xi} \cdot \hat{e}).$$

Indeed, let d_0 be the unit vector perpendicular to the detector plane and pointing from the source position $y(s_0)$ towards the detector (e.g., $d_0 = \dot{y}(s_0)/|\dot{y}(s_0)|$). This implies $\beta(s_0, x) \cdot d_0 > 0$. It is easy to check that

$$(3.20) \quad \hat{\xi} = d_0 \times (\xi \times d_0), \quad \hat{e} = d_0 \times (e \times \beta(s_0, x)).$$

Therefore,

$$(3.21) \quad \hat{e} \cdot \hat{\xi} = (\xi \times d_0) \cdot (e \times \beta(s_0, x)) = (\beta(s_0, x) \cdot d_0)(e \cdot \xi),$$

and (3.19) follows. In (3.21) we have used that $\beta(s_0, x) \cdot \xi = 0$. Similarly,

$$(3.22) \quad \xi \cdot \dot{y}(s_0) = \hat{\xi} \cdot \dot{y}(s_0)$$

because $d_0 \cdot \dot{y}(s_0) = 0$. Combining (3.19) and (3.22) gives

$$(3.23) \quad \text{sgn}(\xi \cdot \dot{y}(s_0)) \text{sgn}(\xi \cdot e(s_0, x)) = \text{sgn}(\hat{\xi} \cdot \dot{y}(s_0)) \text{sgn}(\hat{\xi} \cdot \hat{e}(s_0, x)).$$

For convenience, vectors $\dot{y}(s_0)$ and $\hat{e}(s_0, x)$ are shown in Figure 4.

Let us discuss how $\dot{y}(s_0)$ and $\hat{e}(s_0, x)$ should be drawn in Figure 4. By construction, $\dot{y}(s_0)$ is parallel to the detector plane, that is $d_0 \cdot \dot{y}(s_0) = 0$. Therefore, we should draw $\dot{y}(s_0)$ parallel to L_0 and pointing upward (i.e., $\dot{y}(s_0) \cdot e_3 > 0$). Let e_1 be the unit vector in the direction of the d_1 -axis. Then $e_1 = d_0 \times e_3$ (see Figures 2 and 4) and

$$(3.24) \quad \begin{aligned} \hat{e}(s_0, x) \cdot e_1 &= \{d_0 \times [e(s_0, x) \times \beta(s_0, x)]\} \cdot \{d_0 \times e_3\} = e_3 \cdot [e(s_0, x) \times \beta(s_0, x)] \\ &= e_3 \cdot [(\beta(s_0, x) \times u(s_0, x)) \times \beta(s_0, x)] \\ &= [(\beta(s_0, x) \times u(s_0, x)) \cdot [\beta(s_0, x) \times e_3]] = u(s_0, x) \cdot e_3 > 0, \end{aligned}$$

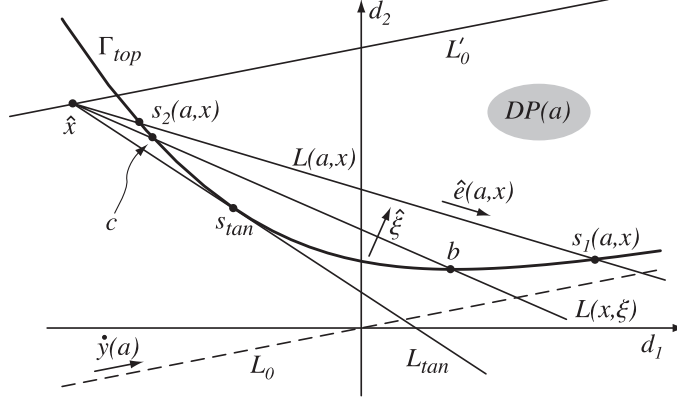
where we have used that $e_3 \cdot d_0 = 0$, $\beta(s_0, x) \cdot u(s_0, x) = 0$ (by construction), and (2.11). Therefore, $\hat{e}(s_0, x)$ should point to the right as shown in Figure 4. Note that if $\hat{x} \in L_0$, then $L(s_0, x) = L_0$, $\hat{e}(s_0, x)$ and $\dot{y}(s_0)$ are parallel and point in the same direction.

To compute $B(x, \xi)$ we have to consider several cases.

I. $\xi \in \Xi_1(x)$. Since in this case $\Pi(x, \xi) \cap C_{PI}(x)$ consists of only one point, say $y(s_0)$, $L(x, \xi) \subset D_1$ and $\text{sgn}(\hat{\xi} \cdot \hat{e}(s_0, x)) = \text{sgn}(\hat{\xi} \cdot \dot{y}(s_0))$. Hence, from (3.8) and

(3.23):

(3.25)
$$B(x, \xi) = \text{sgn}(\xi \cdot \dot{y}(s_0)) \text{sgn}(\xi \cdot e(s_0, x)) = 1, \quad \xi \in \Xi_1(x).$$

FIGURE 6. Top half of the detector plane projected from $y(a)$

II. $\xi \in \Xi_3(x) \setminus \Xi_\psi(x)$. In this case there are three points in $\Pi(x, \xi) \cap C_{PI}(x)$ corresponding to $s_b(x) < a < b < c < s_t(x)$.

II.1. Consider the detector plane $DP(a)$, where a is the smallest value of the parameter among the three points. Since $y(a)$ is the lowest point of intersection and there are two more points in $\Pi(x, \xi) \cap C_{PI}(x)$, the line $L(x, \xi)$ intersects the part of Γ_{top} corresponding to $a < s < s_t(x)$ at two points (see Figure 6).

II.1.a. If $c < s_2(a, x)$, then $L(x, \xi)$ passes between $L(a, x)$ and L_{tan} . This case is illustrated by Figure 6. Consequently,

(3.26)
$$\text{sgn}(\hat{\xi} \cdot \dot{y}(a)) = \text{sgn}(\hat{\xi} \cdot \hat{e}(a, x)) \text{ and } \text{sgn}(\xi \cdot \dot{y}(a)) \text{sgn}(\xi \cdot e(a, x)) = 1.$$

II.1.b. If $c > s_2(a, x)$, then $L(x, \xi)$ passes between $L(a, x)$ and L'_0 . Consequently,

(3.27)
$$\text{sgn}(\hat{\xi} \cdot \dot{y}(a)) = -\text{sgn}(\hat{\xi} \cdot \hat{e}(a, x)) \text{ and } \text{sgn}(\xi \cdot \dot{y}(a)) \text{sgn}(\xi \cdot e(a, x)) = -1.$$

The case $c = s_2(a, x)$ need not be considered because this leads to

(3.28)
$$\{y(s_0), y(s_2), y(s_1(s_0, s_2))\} \in \Pi(x, \xi),$$

which contradicts the assumption $\xi \notin \Xi_\psi(x)$.

II.2. Consider the detector plane $DP(b)$. Since $y(b)$ is the middle point of intersection, $L(x, \xi)$ passes through D_3 because it has to intersect both Γ_{top} and Γ_{bot} at $s = c, b < c < s_t(x)$ and $s = a, s_b(x) < a < b$, respectively. Therefore,

(3.29)
$$\text{sgn}(\hat{\xi} \cdot \dot{y}(b)) = \text{sgn}(\hat{\xi} \cdot \hat{e}(b, x)) \text{ and } \text{sgn}(\xi \cdot \dot{y}(b)) \text{sgn}(\xi \cdot e(b, x)) = 1.$$

II.3. Consider the detector plane $DP(c)$. Since $y(c)$ is the highest point of intersection and there are two more points in $\Pi(x, \xi) \cap C_{PI}(x)$, $L(x, \xi)$ intersects the part of Γ_{bot} corresponding to $s_b(x) < s < c$ at two points.

II.3.a. Suppose the triple $\{a, b, c\}$ is such that case II.1.a occurs. This implies that $L(x, \xi)$ in the $DP(c)$ -plane is between $L(c, x)$ and L'_0 as shown in Figure 7. Indeed, otherwise we get (see Figure 8):

(3.30)
$$s'_2 < a < b < s'_1 = \psi(c - s'_2) + s'_2, \quad s'_2 := s_2(c).$$

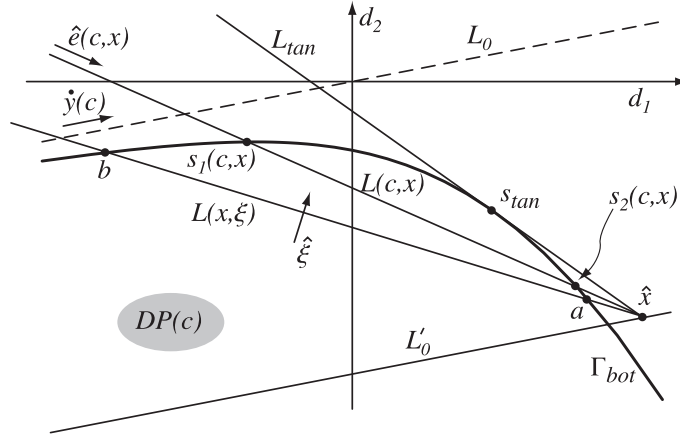


FIGURE 7. Correct location of the line $L(x, \xi)$, which is compatible with case II.1.a. Bottom half of the detector plane is shown

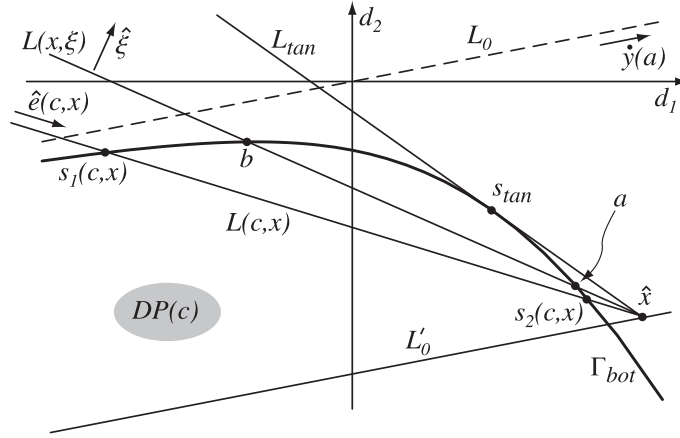


FIGURE 8. The arrangement of lines shown here is incompatible with case II.1.a. Bottom half of the detector plane is shown

Case II.1.a occurs if

$$(3.31) \quad s_1 = a + \psi(s_2 - a) < b < c < s_2, \quad s_2 := s_2(a).$$

From (3.30), (3.31),

$$(3.32) \quad a + \psi(s_2 - a) < \psi(c - s'_2) + s'_2, \quad s'_2 < a < c < s_2.$$

Since $0 < \psi' < 1$,

$$(3.33) \quad a + \psi(s_2 - a) > s'_2 + \psi(s_2 - s'_2) > s'_2 + \psi(c - s'_2),$$

and this contradicts (3.32). Therefore,

$$(3.34) \quad \text{sgn}(\hat{\xi} \cdot \dot{y}(c)) = -\text{sgn}(\hat{\xi} \cdot \hat{e}(c, x)) \text{ and } \text{sgn}(\xi \cdot \dot{y}(c)) \text{sgn}(\xi \cdot e(c, x)) = -1.$$

II.3.b. Suppose the triple $\{a, b, c\}$ is such that the case II.1.b occurs. Analogously, this implies that the image of $L(x, \xi)$ in the $DP(c)$ -plane is between $L(c, x)$

and L_{tan} and

$$(3.35) \quad \text{sgn}(\hat{\xi} \cdot \dot{y}(c)) = \text{sgn}(\hat{\xi} \cdot \hat{e}(c, x)) \text{ and } \text{sgn}(\xi \cdot \dot{y}(c)) \text{sgn}(\xi \cdot e(c, x)) = 1.$$

Let us now summarize. If $\xi \in \Xi_1(x)$, $B(x, \xi) = 1$ from (3.25). If $\xi \in \Xi_3(x) \setminus \Xi_\psi(x)$, there are three points of intersection: $s_b(x) < a < b < c < s_t(x)$. Contribution of the middle point $y(b)$ to the sum in (3.8) equals one, and contributions of the points $y(a), y(c)$ cancel each other (see (3.26) and (3.34), (3.27) and (3.35)). Since the sets $Crit(x)$ and $\Xi_\psi(x)$ have measure zero, the proof is finished.

4. PRACTICAL IMPLEMENTATION AND NUMERICAL EXPERIMENTS

In this section we discuss efficient implementations of inversion formulas (2.13) and (2.14). Consider (2.13) first. It is clear from (2.12) that $s_2(s, x)$ actually depends only on s and $\beta(s, x)$. Therefore, we can write

$$(4.1) \quad \begin{aligned} u(s, \beta) &:= u(s, s_2(s, \beta)), \quad e(s, \beta) := \beta \times u(s, \beta), \quad \beta \in S^2, \\ \Psi(s, \beta) &:= \int_0^{2\pi} \frac{\partial}{\partial q} D_f(y(q), \cos \gamma \beta + \sin \gamma e(s, \beta)) \Big|_{q=s} \frac{1}{\sin \gamma} d\gamma, \\ f(x) &:= -\frac{1}{2\pi^2} \int_{I_{PI}(x)} \frac{1}{|x - y(s)|} \Psi(s, \beta(s, x)) ds. \end{aligned}$$

Fix $s_2 \in [s - 2\pi + \Delta, s + 2\pi - \Delta]$, $s_2 \neq s$, and let $\Pi(s_2)$ denote the plane through $y(s), y(s_2)$, and $y(s_1(s, s_2))$. If $s_2 = s$, $\Pi(s_2)$ is determined by continuity and coincides with the plane through $y(s)$ and parallel to $\dot{y}(s), \ddot{y}(s)$. The family of lines $L(s_2)$ obtained by intersecting $\Pi(s_2)$ with the detector plane is shown in Figure 4. By construction, given any $x \in U$ with $\beta(s, x)$ parallel to $\Pi(s_2)$, s_2 used here is precisely the same as s_2 found by solving (2.12). Since $e(s, \beta) \cdot \beta = 0$, $|e(s, \beta)| = 1$, we can write (with abuse of notation):

$$(4.2) \quad \beta = (\cos \theta, \sin \theta), \quad e(s, \beta) = (-\sin \theta, \cos \theta), \quad \beta, e(s, \beta) \in \Pi(s_2).$$

Therefore,

$$(4.3) \quad \Psi(s, \beta) = \int_0^{2\pi} \frac{\partial}{\partial q} D_f(y(q), (\cos(\theta + \gamma), \sin(\theta + \gamma))) \Big|_{q=s} \frac{1}{\sin \gamma} d\gamma, \quad \beta \in \Pi(s_2).$$

Equation (4.3) is of convolution type and one application of Fast Fourier Transform (FFT) gives values of $\Psi(s, \beta)$ for all $\beta \in \Pi(s_2)$ at once.

Equations (4.1) and (4.3) imply that the resulting algorithm is of the filtered-backprojection type. First, one computes shift-invariant filtering of a derivative of cone beam projections using (4.3) for all $s_2 \in [s - 2\pi + \Delta, s + 2\pi - \Delta]$ (cf. Figure 4). The second step is backprojection according to (4.1). Since $\partial/\partial q$ in (4.1) and (4.3) is a local operation, each cone beam projection is stored in memory as soon as it has been acquired for a short period of time for computing this derivative at a few nearby points and is never used later.

Comparing (2.13) and (2.14) we see that (2.14) admits absolutely analogous filtered-backprojection implementation. Moreover, since no derivative with respect to the parameter along the spiral is present, there is never a need to keep more than one cone beam projection in computer memory at a time.

Consider now the requirements on the detector array imposed by the algorithm. Clearly, they depend on the function ψ in (2.6). In the experiments described below $\psi(t) = t/2$ and $s_1(s_0, s_2)$ is given by (2.8). From the discussion preceding (4.2) we

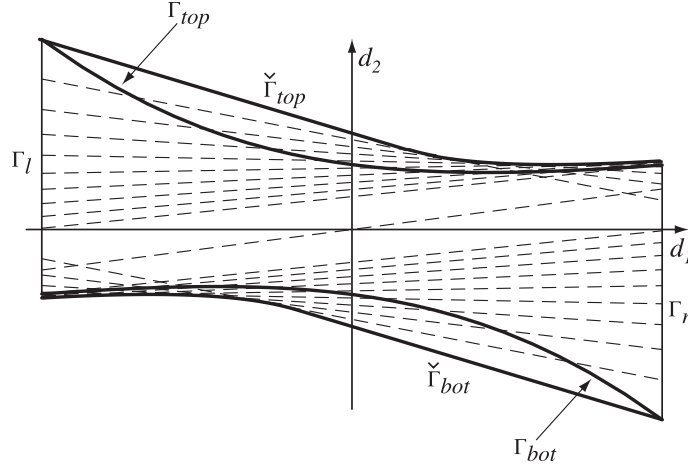


FIGURE 9. Dashed segments are segments of lines $L(s_2)$ located between Γ_l and Γ_r

conclude that given any line $L(s_2)$, $s_2 \in [s - 2\pi + \Delta, s + 2\pi - \Delta]$, its segment located between Γ_l and Γ_r should be inside the detector array. These segments are shown in Figure 9. Thus, the left and right boundaries of the required detector array are still Γ_l and Γ_r , but the new top and bottom boundaries are determined using the envelopes of the lines $L(s_2)$. In Figure 9 these boundaries are denoted $\check{\Gamma}_{top}$ and $\check{\Gamma}_{bot}$. As is seen, the detector array required for the algorithm (its area is denoted A_{alg}) is not much greater than the theoretically minimum one. The latter is bounded by Γ_{top} and Γ_{bot} and its area is denoted A_{min} . The ratio of the areas A_{alg}/A_{min} grows as $r/R \rightarrow 1$, but slowly. For example, $A_{alg}/A_{min} = 1.209, 1.230, \text{ and } 1.255$ when $r/R = 0.5, 0.6, \text{ and } 0.7$, respectively. The case $r/R = 0.7$ is shown in Figure 9. For comparison note that if $r/R = 0.5$ the algorithm of [Kat01b, Kat01a] requires a detector array with area $1.93 A_{min}$.

Consider $L(s_2)$ corresponding to the largest possible value $s_2 = s + 2\pi - \Delta$ (cf. Figure 3). Since $s_1 = (s + s_2)/2 = s + \pi - \Delta/2 < s + \pi$, this line intersects Γ_{top} to the right of the d_2 -axis and, therefore, intersects Γ_r above the point corresponding to $s_2 = s - 2\pi + \Delta$. Hence, the entire segment of this line located between Γ_l and Γ_r is inside the detector array and there is no restriction on how big the set U can be inside the spiral as long as $r/R < 1$. This is in contrast with the inversion algorithm proposed in [Kat01b] (see also [Kat01a]). In the earlier algorithm one has to know the cone beam data along all lines tangent to Γ_{top} and Γ_{bot} at points between Γ_l and Γ_r . Therefore, if r/R is close to one (Δ is close to zero), the line tangent to Γ_{top} at $s_{tan} = s + 2\pi - \Delta$ intersects Γ_r below the point corresponding to $s - 2\pi + \Delta$, thereby increasing significantly the required detector array.

Consider now three numerical experiments. Parameters of the data collection protocols are given in Table 1. Reconstructions in Experiment 1 are done using (2.13), and reconstructions in Experiments 2 and 3 are done using (2.14). The axial span of the detector array in Experiment 2 is slightly bigger than that in Experiment 1 (despite h being equal in both cases) because to use (2.14) we need a little extra space for computing derivatives of the data with respect to the angular variables.

Experiment number	1	2	3
R (radius of the spiral)	3		
h (pitch of the spiral)	0.5	0.5	1.0
axial span of the detector array	0.70	0.72	1.44
transverse span of the detector array	4.26		
number of detector rows	50	50	200
number of detectors per row	500		
number of source positions per one turn of the spiral	1500	1000	1000

TABLE 1. Parameters of the data collection protocols

Results of Experiments 1, 2, and 3 are shown in Figures 10, 11, and 12, respectively. Left panels of these figures show the 3-D low contrast Shepp phantom (see Table 1 in [KMS98]). Top half demonstrates a vertical slice through the reconstructed image at $x_1 = -0.25$, and bottom half - the graphs of exact (dashed line) and computed (solid line) values of f along a vertical line $x_1 = -0.25, x_2 = 0$. We used the grey scale window $[1.01, 1.03]$ to make low-contrast features visible. Right panels of these figures show the disk phantom, which consists of six identical flattened ellipsoids (lengths of half-axes: 0.75, 0.75, and 0.04, distance between centers of neighboring ellipsoids: 0.16). Again, top half demonstrates a vertical slice through the reconstructed image at $x_1 = 0$, and the bottom half - the graphs of exact (dashed line) and computed (solid line) values of f along a vertical line $x_1 = 0, x_2 = 0$.

REFERENCES

- [B⁺00] H. Bruder et al., *Single slice rebinning reconstruction in spiral cone-beam computed tomography*, IEEE Transactions on Medical Imaging **19** (2000), 873–887.
- [D⁺97] P. E. Danielsson et al., *Towards exact reconstruction for helical cone-beam scanning of long objects. A new detector arrangement and a new completeness condition*, Proc. 1997 Meeting on Fully 3D Image Reconstruction in Radiology and Nuclear Medicine (Pittsburgh) (D. W. Townsend and P. E. Kinahan, eds.), 1997, pp. 141–144.
- [DNK00] M. Defrise, F. Noo, and H. Kudo, *A solution to the long-object problem in helical cone-beam tomography*, Physics in Medicine and Biology **45** (2000), 623–643.
- [Kat01a] A. Katsevich, *An inversion algorithm for Spiral CT*, Proceedings of the 2001 International Conference on Sampling Theory and Applications, May 13–17, 2001, University of Central Florida (A. I. Zayed, ed.), 2001, pp. 261–265.
- [Kat01b] A. Katsevich, *Theoretically exact FBP-type inversion algorithm for Spiral CT*, (submitted).
- [Kat02] A. Katsevich, *Microlocal analysis of an FBP algorithm for truncated spiral cone beam data*, Journal of Fourier Analysis and Applications (2002), (to appear).
- [KMS98] H. Kudo, N. Miyagi, and T. Saito, *A new approach to exact cone-beam reconstruction without Radon transform*, 1998 IEEE Nuclear Science Symposium Conference Record, IEEE, 1998, pp. 1636–1643.
- [KND98] H. Kudo, F. Noo, and M. Defrise, *Cone-beam filtered-backprojection algorithm for truncated helical data*, Phys. Med. Biol. **43** (1998), 2885–2909.
- [KS97] H. Kudo and T. Saito, *An extended cone-beam reconstruction using Radon transform*, 1996 IEEE Med. Imag. Conf. Record, IEEE, 1997, pp. 1693–1697.
- [KSK00] M. Kachelriess, S. Schaller, and W. A. Kalender, *Advanced single-slice rebinning in cone-beam spiral CT*, Medical Physics **27** (2000), 754–772.
- [Lan93] S. Lang, *Real and functional analysis*, 3rd ed., Springer-Verlag, New York, 1993.

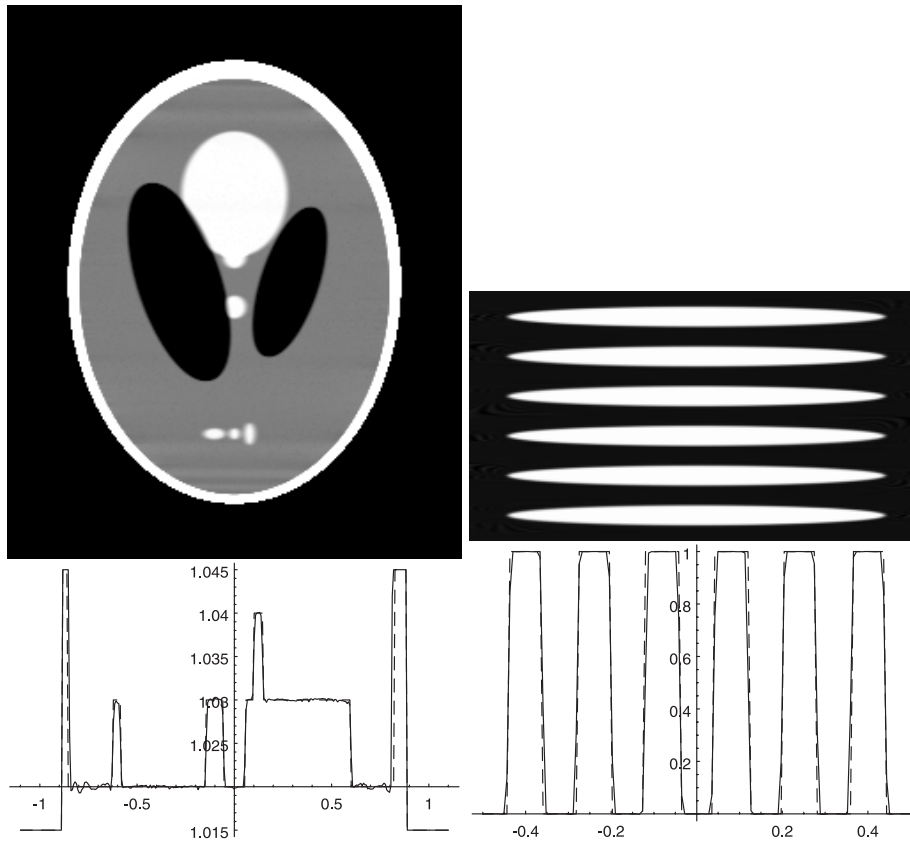


FIGURE 10. Experiment 1: Reconstruction formula (2.13), $h = 0.5$

- [NKD98] F. Noo, H. Kudo, and M. Defrise, *Approximate short-scan filtered-backprojection for helical CB reconstruction*, Conf. Rec. 1998 IEEE Nuclear Science Symposium (Toronto, Ont., Canada), vol. 3, IEEE, Piscataway, NJ, 1998, pp. 2073–2077.
- [SNS⁺00] S. Schaller, F. Noo, F. Sauer, et al., *Exact Radon rebinning algorithm for the long object problem in helical cone-beam CT*, IEEE Trans. on Medical Imaging **19** (2000), 361–375.
- [Tam95] K. C. Tam, *Method and apparatus for converting cone beam x-ray projection data to planar integral and reconstructing a three-dimensional computerized tomography (CT) image of an object*, US Patent 5,257,183, October 1995.
- [Tam97] K. C. Tam, *Cone-beam imaging of a section of a long object with a short detector*, Information processing in medical imaging (J. S. Duncan and G. R. Gindi, eds.), Lecture Notes in Computer Science, vol. 1230, Springer, Berlin, 1997, pp. 525–530.
- [TD00] H. Turbell and P.-E. Danielsson, *Helical cone beam tomography*, Int. J. of Imaging Syst. and Technology **11** (2000), 91–100.

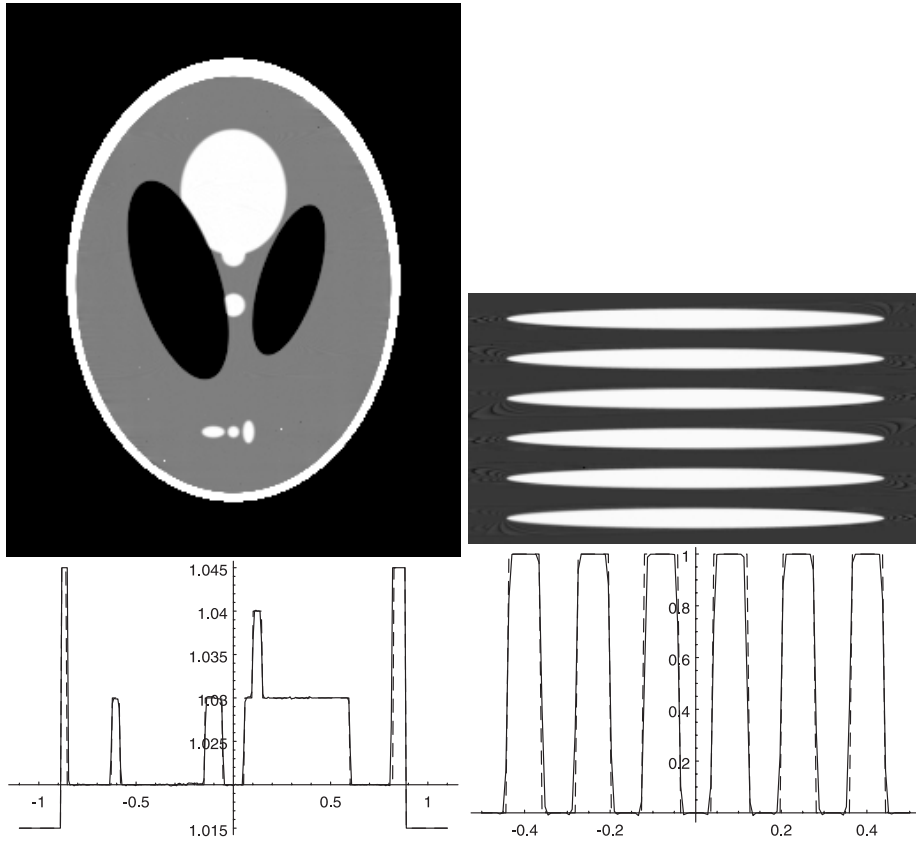


FIGURE 11. Experiment 2: Reconstruction formula (2.14), $h = 0.5$

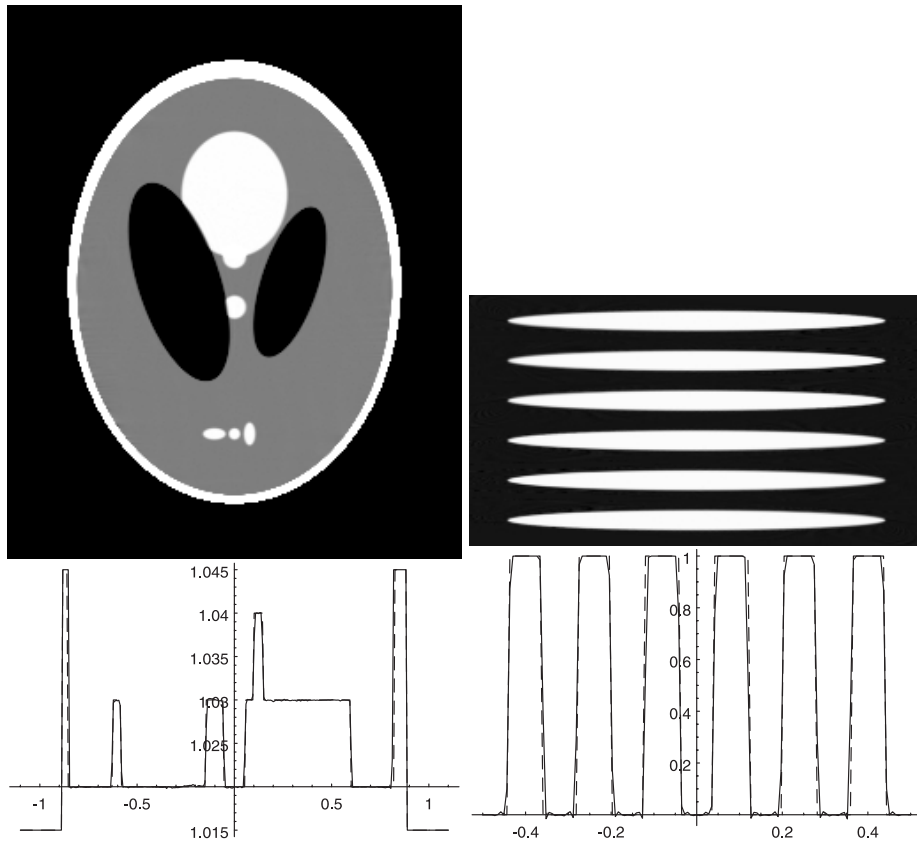


FIGURE 12. Experiment 3: Reconstruction formula (2.14), $h = 1.0$